catalysts

MDPI

Article

Mechanistic Study of Silane Alcoholysis Reactions with Self-Assembled Monolayer-Functionalized Gold Nanoparticle Catalysts

Katsuhiro Isozaki [1,2,3,*], Tomoya Taguchi [3,4], Kosuke Ishibashi [1,2], Takafumi Shimoaka [1], Wataru Kurashige [5], Yuichi Negishi [5], Takeshi Hasegawa [1], Masaharu Nakamura [1,2] and Kazushi Miki [3,4,6,*]

1 Institute for Chemical Research, Kyoto University, Gokasyo, Uji, Kyoto 611-0011, Japan; pj.en.omocod.kyoa@gmail.com (K.I.); shimoaka@scl.kyoto-u.ac.jp (T.S.); htakeshi@scl.kyoto-u.ac.jp (T.H.); masaharu@scl.kyoto-u.ac.jp (M.N.)
2 Department of Energy and Hydrocarbon Chemistry, Graduate School of Engineering, Kyoto University, Nishikyoku, Kyoto 615-8510, Japan
3 National Institute for Materials Science, 1-1 Namiki, Tsukuba, Ibaraki 305-0044, Japan; ntscp2020@gmail.com
4 Department of Pure and Applied Sciences, University of Tsukuba, 1-1-1 Tennodai, Tsukuba, Ibaraki 305-8571, Japan
5 Department of Applied Chemistry, Faculty of Science, Tokyo University of Science, 1-3 Kagurazaka, Shinjuku-ku, Tokyo 162-8601, Japan; wataru.kurashige0414@gmail.com (W.K.); negishi@rs.kagu.tus.ac.jp (Y.N.)
6 Department of Electrical Materials and Engineering, Graduate School of Engineering, University of Hyogo, Shosya 2167, Himeji, Hyogo 671-2280, Japan
* Correspondence: kisozaki@scl.kyoto-u.ac.jp (K.I.); miki@eng.u-hyogo.ac.jp (K.M.)

Received: 13 July 2020; Accepted: 7 August 2020; Published: 9 August 2020

Abstract: The self-assembled monolayer (SAM)-modified metallic nanoparticles (MNPs) often exhibit improved chemoselectivity in various catalytic reactions by controlling the reactants' orientations adsorbed in the SAM; however, there have been a few examples showing that the reaction rate, i.e., catalytic activity, is enhanced by the SAM-modification of MNP catalysts. The critical parameters that affect the catalytic activity, such as the supports, nanoparticle size, and molecular structures of the SAM components, remain uninvestigated in these sporadic literature precedents. Here, we report the mechanistic investigation on the effects of those parameters on the catalytic activity of alkanethiolate SAM-functionalized gold nanoparticles (AuNPs) toward silane alcoholysis reactions. The evaluation of the catalytic reaction over two-dimensionally arrayed dodecanethiolate SAM-functionalized AuNPs with different supports revealed the electronic interactions between AuNPs and the supports contributing to the rate enhancement. Additionally, an unprecedented size effect appeared—the AuNP with a 20 nm radius showed higher catalytic activity than those at 10 and 40 nm. Infrared reflection–absorption spectroscopy revealed that the conformational change of alkyl chains of the SAM affects the entrapment of reactants and products inside the SAM, and therefore brings about the acceleration effect. These findings provide a guideline for further applying the SAM-functionalization technique to stereoselective organic transformations with designer MNP catalysts.

Keywords: gold nanoparticle; catalysts; self-assembled monolayer; silane alcoholysis; size effect; support effect; molecular recognition; IR reflection-absorption spectroscopy

1. Introduction

Metallic nanoparticles (MNPs) have been emerging as a promising catalyst in chemical synthesis over the last two decades due to their remarkable catalytic activities and selectivities in various reactions [1–3]. The typical approach for tuning the catalytic activity and selectivity of MNPs is to change their size and supports, which varies the number of surface atoms and the type of contact atoms in the catalytically active sites of MNPs [4–13]. Another approach uses a surface modifier, in which a partial coverage of the catalyst surface with a small amount of a modifier is the key to improving the catalytic activity and selectivity. A large amount of strong surface-binding modifiers, on the other hand, suppress the catalytic activity as catalyst poisoning [14–18]. Recently, there has emerged a different approach of functionalizing the whole catalyst surface with self-assembled monolayers (SAMs) to improve the catalyst properties of MNPs [19–28].

Medlin et al. first reported an improved chemoselectivity in the hydrogenation of propylene oxide by the surface functionalization of palladium nanoparticles with the alkanethiolate SAM [24]. Several studies followed this work and described the chemoselective SAM-modified MNP-catalyzed hydrogenation and hydrodeoxygenation using alkanethiolates, alkylamines, and alkyl carboxylates as the modifiers [25–28]. Such chemoselectivity was attributed to the suppression of planar horizontal adsorption of the reactant molecules by capping the MNP surface with the SAM and the intermolecular interactions between the SAM and the reactant molecules [21–28]. These studies investigated the effect of the molecular structure of modifiers forming SAM on the chemoselectivity, yet the effect of nanoparticle size [22,23] and supports on the reactivity and selectivity remains virtually uninvestigated, despite the importance of these parameters in MNP catalysis.

Besides, we found a new phenomenon of reaction acceleration by alkanethiolate SAM-coated gold nanoparticles (AuNPs) catalysts, in which the intermolecular interaction between the SAM and reactant molecules accelerated a silane alcoholysis reaction [29]. While the chemoselectivity increased but the rate of the desired reaction unchanged in the hydrogenation reactions described above, the reaction rate was increased by a SAM-coating in our silane alcoholysis. Meanwhile, in the case of SAM-coated 10 nm AuNP catalysts, the intermolecular interaction between the SAM and reactant molecules has a significant effect on the acceleration of the reaction of silane alcoholysis. Thus, the SAM-functionalization method should be a powerful tool for developing new MNP catalysts with not only chemoselectivity, but also high catalytic activity. Similar to the SAM effect for improving the chemoselectivity of MNP catalysts, it remains unknown how the structural components of MNP catalysts affect the reaction acceleration with the SAM.

Here, we report a mechanistic investigation on the rate acceleration of silane alcoholysis catalyzed by alkanethiolate SAM-functionalized AuNP catalysts (Figure 1). A comparison of the catalytic activities of various SAM-functionalized AuNP-arrays comprising different structural components revealed the origin of the unexpected reaction rate enhancement when using the SAM on AuNPs of intermediate sizes (ca 20 nm). The electronic interaction between the AuNPs and the supports was also found to enhance the catalytic activity of AuNP catalysis. Moreover, the reaction mechanism at the surface of SAM-functionalized AuNPs is discussed through the catalytic reactions via Si–H activation and infrared reflection–absorption (IR RA) measurements before and after the catalytic silane alcoholysis reaction on SAM-coated Au films.

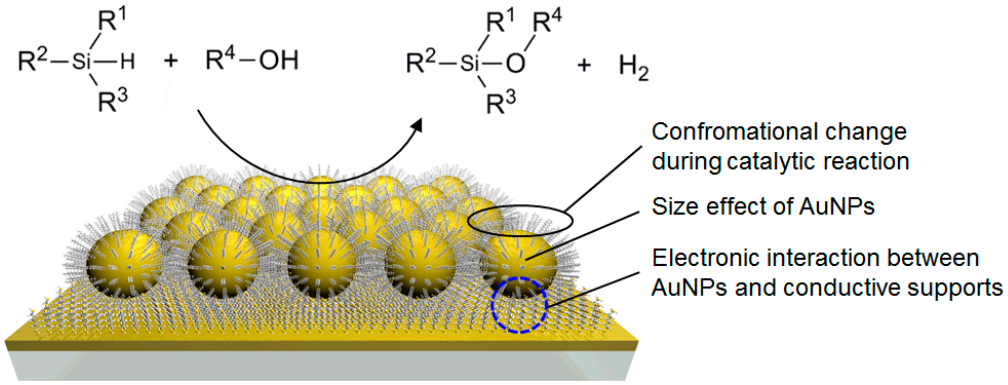

Figure 1. Schematic structure of the alkanethiolate self-assembled monolayer (SAM)-functionalized gold nanoparticle (AuNP) catalysts supported on conductive films for a silane alcoholysis reaction.

2. Results and Discussion

2.1. Fabrication of Alkanethiolate SAM-Functionalized AuNP-Arrays

A series of AuNPs were synthesized according to the reported methods [30,31]. AuNPs with diameters of 5 and 10 nm were synthesized by the seed-mediated growth method, in which ca 3.5 nm AuNP seed was synthesized by the reduction of $HAuCl_4$ with $NaBH_4$ in the presence of citrate, then the growth reaction took place by adding $HAuCl_4$, cetyltrimethylammonium bromide and ascorbic acid with the reported ratio [30]. For the larger AuNPs with a diameter of 20 and 40 nm, Frens' method was used [31]. An aqueous solution of trisodium citrate was added into a boiled aqueous solution of $HAuCl_4$ at once with the reported ratio. The obtained AuNPs were characterized by TEM and SEM to have diameters of 5.8 ± 0.1, 10.8 ± 0.1, 21.2 ± 0.3, and 40.8 ± 1.0 nm, respectively (Figures S2–S5). The characteristic localized surface plasmon resonance (LSPR) peaks of these AuNPs were observed by UV-Vis absorption spectra at 518, 520, 522, and 534 nm, respectively (Figures S2–S5). A commercial 9 nm AuNP was used according to the previous report [29,32–34]. The surface of these AuNPs with diameters of 5.8 ± 0.1, 9.0 ± 0.2, 10.8 ± 0.1, 21.2 ± 0.3, and 40.8 ± 1.0 nm was functionalized with dodecanethiol in colloidal states to afford a series of dodecanethiolate-coated AuNPs (designated as **5Dod-AuNP, 9Dod-AuNP, 10Dod-AuNP, 20Dod-AuNP,** and **40Dod-AuNP**, respectively) [35]. SEM observations revealed the negligible change in the size and morphology of AuNPs by a functionalization with thiols (Figures S2–S5). These AuNPs were immobilized into 2D-arrays on 1 cm × 1 cm Au-spattered quartz plates using our reported method [32–34] to give **5Dod-array, 9Dod-array, 10Dod-array, 20Dod-array,** and **40Dod-array**. Dodecanethiolate-coated 10 nm AuNP-arrays on Cr- and indium tin oxide (ITO)-spattered quartz plates were fabricated and designated as the 10Dod-array/Cr and **10Dod-array/ITO**, respectively. SEM observations revealed the regularly arrayed AuNP structures, and the coverage of AuNP-arrays on the support was determined by averaging measurements made at seven different locations on each plate (Figure 2), similar to our previous report [34]. In most cases, the high coverage of AuNP-arrays was achieved on the Au film supports except for the 40Dod-array (Figure 2d), in which the interparticle interaction was too strong to form a uniformly dispersed 2D array [32]. The **10Dod-array/Cr** and **10Dod-array/ITO** had lower coverages of 21% and 24% (Figure 2e,f), respectively, under the fabrication condition optimized for Au-spattered quartz plates [34].

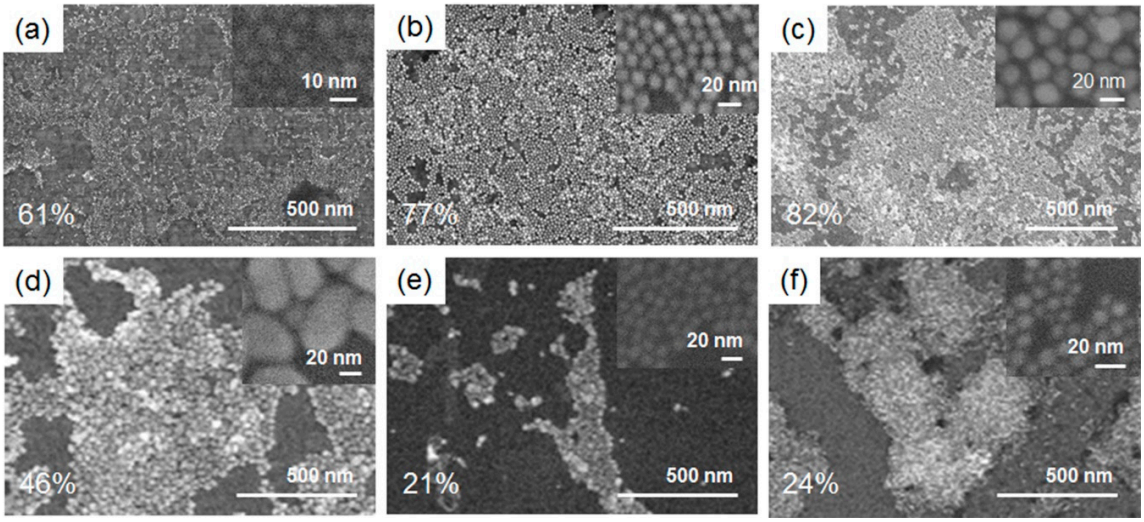

Figure 2. SEM images of the (**a**) **5Dod-array**, (**b**) **10Dod-array**, (**c**) **20Dod-array**, (**d**) **40Dod-array**, (**e**) **10Dod-array/Cr**, and (**f**) **10Dod-array/ indium tin oxide** (ITO). Inset shows magnified SEM images.

2.2. *Effect of AuNP Coverage on the Support*

In order to investigate the relationship between the coverage of AuNPs on the support and the catalytic activity of SAM-capped AuNP-arrays, a catalytic alcoholysis reaction of dimethylphenylsilane (DMPS) with butanol was carried out using the **10Dod-array** with a coverage of 2–95% (Figure 3), fabricated by changing the concentration of the **10Dod-AuNP** colloidal solution. The yields of the silylether product, DMPS–OBu, after a 1 h reaction vs. The coverage of the **10Dod-array** are plotted in Figure 3. Although the reaction yield depends linearly on the coverage between 2 and 70%, it gradually becomes saturated at around 70% coverage. This result suggests that the number of surface gold atoms exposed to the reaction solution on a given AuNP is almost the same as 70% coverage, and then it gradually decreases due to the dense packing of AuNPs to form AuNP-arrays. SEM observations revealed that **10Dod-AuNP** forms small islands of AuNP-arrays even at lower coverages, as can be seen in the samples of **10Dod-array/Cr** and **10Dod-array/ITO** (Figure 2e,f). Thus, a coverage of 70% is considered the critical point for forming large AuNP-arrays from small islands of them.

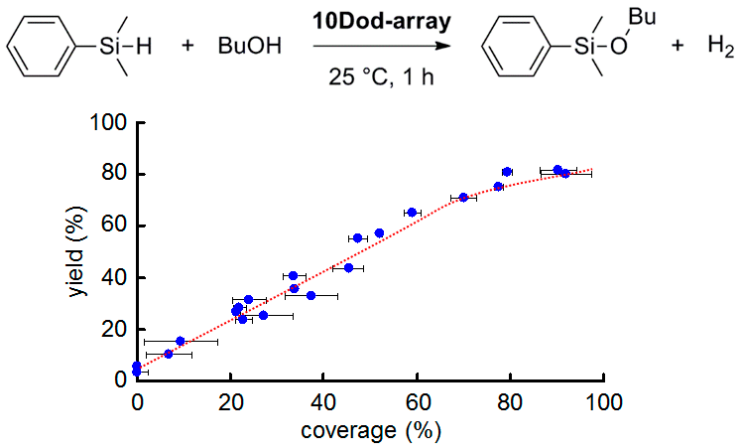

Figure 3. AuNP coverage dependent catalytic activity of the **10Dod-array**. Reaction condition: dimethylphenylsilane (DMPS) (150 μmol) in BuOH (3.0 mL) at 25 °C for 1 h.

2.3. Effect of the Support

Previously, we ascribed the high catalytic activity of alkanethiolate SAM-functionalized AuNPs to two different effects, the reaction acceleration with the SAMs and the immobilization of AuNPs onto the conductive film supports [8]. It is well known that the supports for MNP catalysts affect the catalytic performance, because the atom–atom contacts at the nanoparticle–support interface create perimeter atoms acting as the catalytic active sites [2–5]. In the present SAM-functionalized AuNP-arrays, the AuNPs were covalently immobilized on the conductive film supports through a 1,6-hexanedithiolate monolayer, and thus it was unclear how the non-contacting supports affect the catalytic activity of the AuNP-arrays. In order to investigate this effect in SAM-functionalized AuNP-arrays, 10Dod-arrays were fabricated on three metallic films of gold, chromium, and ITO (**10Dod-array**, **10Dod-array/Cr**, and **10Dod-array/ITO**, respectively). SEM observations revealed the coverage of the **10Dod-array/Cr** and **10Dod-array/ITO** to be 21% and 24%, respectively (Figure 2e,f), while the **10Dod-array** on the Au support had a higher coverage of 38% in this experiment. The catalytic activities of these AuNP-arrays were evaluated by the alcoholysis reaction of DMPS with BuOH. The initial reaction rate in each case was calculated from pseudo-first order kinetics of the initial reaction steps and is summarized in Table 1 (Figure S6). The amount of surface Au atoms was estimated based on the coverage in a way similar to our previous paper [29], and the initial reaction rate per surface Au atom of 10Dod-arrays on Au, Cr, and ITO supports was calculated to be 7.60, 16.6, and 32.4 × 10^6 min^{-1} mol^{-1} (Table 1 entries 1–3, Figure 4), respectively. This tendency roughly coincides with the respective work functions of Au, Cr, and ITO of 5.3, 4.5 [36], and ca 4.3 eV [37]. A lower work function is correlated to a higher catalytic activity (Figure 4), suggesting that charge transfers from the conductive film supports to the AuNPs accelerated the silane alcoholysis reaction. It is noteworthy that the reference systems of 1,6-hexanedithiolate SAM-coated Au, Cr, and ITO supports without AuNPs showed almost no reactivity for the same reaction [38]. Therefore, the metallic film supports themselves do not have catalytic activity, and the electronic interaction between the AuNPs and the supports through the monolayer of 1,6-hexanedithiolate plays an important role in accelerating the AuNP-catalyzed reaction.

Table 1. Various AuNP-array-catalyzed butanolyses of DMPS [a].

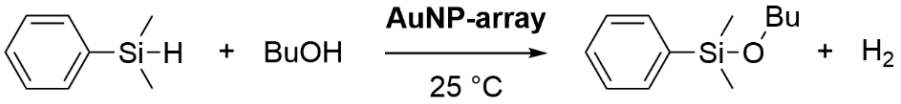

Entry	Catalyst	Coverage (%)	Yield (%) [b]	Initial Reaction Rate (×10^{-4} min^{-1})	Effective Surface Au Atom (nmol)	Initial Reaction Rate/Effective Surface Au Atom (×10^6 min^{-1} mol^{-1})
1	**10Dod-array**	38	38	78.0	1.02	7.60
2	**10Dod-array/Cr**	21	44	94.0	0.56	16.6
3	**10Dod-array/ITO**	24	76	210	0.65	32.4
4	**5Dod-array**	84	61	176	1.63	10.8
5 [c]	**9Dod-array**	90	83	147	2.07	7.15
6	**20Dod-array**	47	50	152	1.56	9.72
7	**40Dod-array**	74	58	145	2.75	5.27

[a] Reaction condition: DMPS (150 μmol) in BuOH (3.0 mL) with AuNP-array catalysts at 25 °C. [b] Yield at 1 h. [c] Ref. [29].

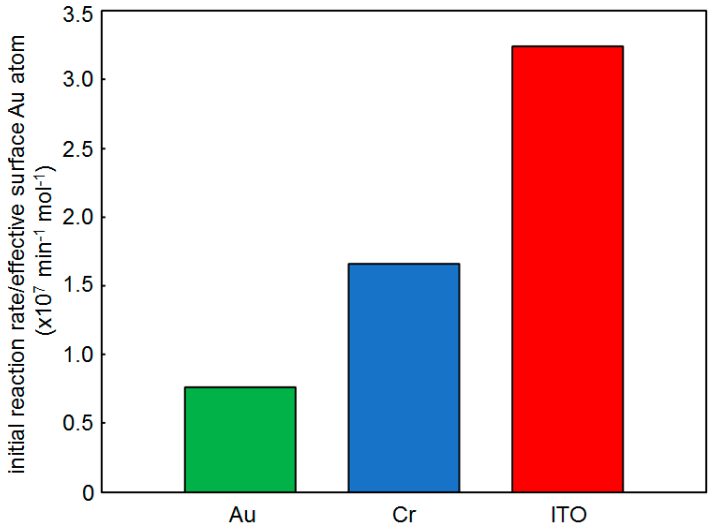

Figure 4. Catalytic activity of the 10Dod-array with different supports.

2.4. Investigation for Reactive Intermediates on the AuNP Surface

A ^{1}H NMR analysis was used to obtain insights into the reaction mechanism. The reaction solution of DMPS was prepared using CD_3OD as an alcohol in the presence of a dispersed colloidal **10Dod-AuNP** catalyst (0.1 mol % of Au atoms) and was monitored by time-course ^{1}H NMR measurements (Figure 5). Soon after starting the reaction by adding DMPS to the solution, new peaks appeared at 0.35 and 4.56 ppm (Figure 5b,c). The singlet signal at 0.35 ppm was assigned to the Si–Me proton of the silylether product $Me_2PhSi–OCD_3$, and its yield was also equal to the consumption of DMPS. The other singlet signal at 4.56 ppm was assigned to molecular hydrogen [39], with an integrated area of 0.79 H compared to that of 6.0 H for Si–Me protons in $Me_2PhSi–OCD_3$, indicating the generation of equimolar monodeuterated hydrogen, HD and the alcoholysis product. After 90 min of reaction, the ^{1}H NMR spectrum showed that 2.4% product was formed together with 1.9% HD. The formation of molecular hydrogen with equimolar silylether reveals that the alcoholysis reaction simply proceeds as depicted in the equation in Figure 5, and the HD is generated from the Si–H hydrogen of DMPS and the deuterium of CD_3OD. In addition, during the reaction, no detachment of thiolates was observed (Figure S7), suggesting the retaining of the SAM structure of thiolates at the AuNP surface.

The reactive intermediate generated on the surface of AuNPs was investigated by tracing the reaction of hydrosilane or alcohol alone in the presence of AuNPs. In the control reaction with only alcohol, **10Dod-AuNP** was mixed with BuOH and stirred at 25 °C. Even after 10 days, this mixture showed a negligible change in both gas chromatography (GC) analysis and ^{1}H NMR measurements. Furthermore, a small amount of acetone was added to the reaction mixture (1/60 eq to BuOH) to check whether the Meerwein–Ponndorf–Verley reduction [40] proceeded, but no reaction could be confirmed by GC analysis after 2 days. These results confirmed that the surface of SAM-coated AuNPs has no reactivity towards alcohol. In the other control reaction with only hydrosilane, a slow consumption of the hydrosilane and the formation of products were observed. After stirring the **10Dod-AuNP** solution in DMPS for 242 h, the ^{1}H NMR spectrum indicated 65% consumption of DMPS and formation of the corresponding silanol and disiloxane in 31% and 29% yields, respectively (Equation (1)). These products are

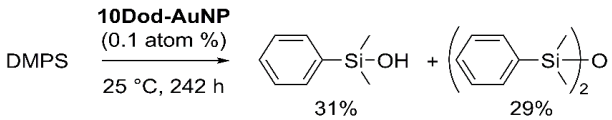

(1)

considered to come from the reaction of DMPS with water that slowly infiltrated the sealed reaction vessel from the atmosphere.

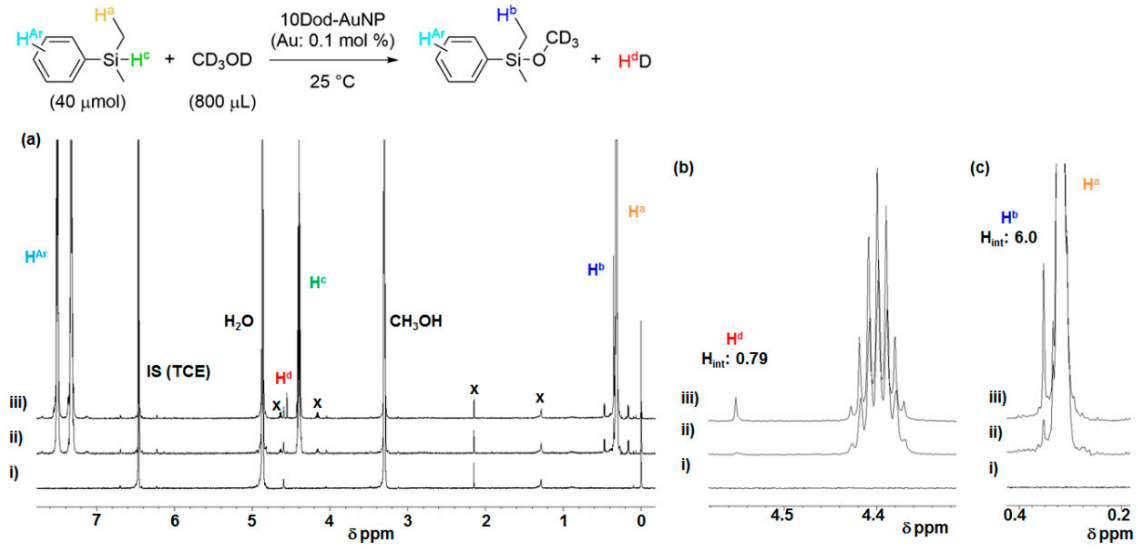

Figure 5. (**a**) Full scale and (**b**), (**c**) magnified ^{1}H NMR spectra (400 MHz) of the silane alcoholysis reaction solution in CD_3OD. (i) Before the addition of DMPS, (ii) 15 min and (iii) 90 min after the addition of DMPS.

Furthermore, to confirm the activation of the Si–H bond on the surface of SAM-functionalized AuNPs, the hydrosilylation of aldehydes was examined. Benzaldehyde (25 mmol) was mixed with DMPS (83 μmol) and the mixture was stirred at 25 °C after adding the **10Dod-array** (coverage: 93%). The reaction was complete after 11 h, and the silylether product, benzyloxydimethylphenylsilane, was obtained in a 54% yield (Equation (2)).

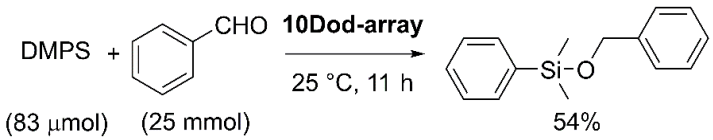

(2)

These results strongly suggest that the hydrosilanes are activated at the surface of AuNPs, and the following catalytic reaction with alcohols or aldehydes gives silylethers as products. Recently, Kaneda et al. reported that the Si–H bond of hydrosilane is cleaved at first, and the following reaction takes place at the surface of hydroxyapatite-supported AuNPs [41,42], which supports our results. A similar reaction mechanism was proposed by Bhattacharjee and Datta based on a density functional theory (DFT) calculation, in which the graphene-supported Au_{16} cluster catalyzes the formation of disiloxane from DMPS and water through the oxidative addition of DMPS to Au_{16}, followed by the adsorption and O–H cleavage of water [43]. Importantly, they found that the turnover-limiting step is the O–H bond cleavage of water, which is accelerated by the charge transfer from graphene to Au_{16}, analogous to the observed support effect in our reaction system. Therefore, a similar reaction mechanism is expected for our system: starting from the oxidative addition of DMPS to SAM-coated AuNPs, the charge transfer from the support then facilitates the O–H bond cleavage of alcohol to give the silylether products (Figure 6).

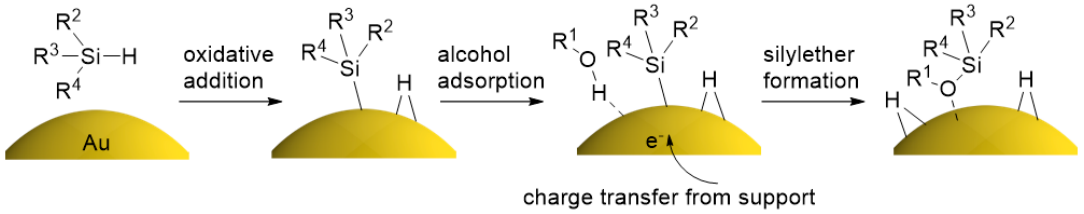

Figure 6. Plausible mechanism of the silane alcoholysis on the AuNP surface accelerated by the charge transfer from support.

2.5. *Effect of AuNP Size*

The nanoparticle (NP) size is known as a key parameter in MNP catalysts, and thus it has been well studied with solid-supported AuNPs [4–9,44–47]. However, the size effect of SAM-coated MNPs remains unexplored. In order to investigate this, gold nanoclusters (AuNCs), having precise molecular formulas such as dodecanethiolate-functionalized Au_{25} ($Octyl_4N[Au_{25}(SDod)_{18}]$) [48–51], Au_{38} ($Au_{38}(SDod)_{24}$) [52–55], glutathione-functionalized Au_{25} ($Na[Au_{25}(SG)_{18}]$) [56,57] nanoclusters, and a series of dodecanethiolate SAM-functionalized AuNP-arrays (**5Dod-array**, **9Dod-array**, **10Dod-array**, **20Dod-array**, and **40Dod-array**), were prepared.

The size-dependent catalytic activity of alkanethiolate-coated AuNPs with cores below 2 nm [58] was investigated by the silane alcoholysis reaction with AuNCs in a homogeneous solution (Figure 7). The dodecanethiolate-functionalized Au_{38} nanocluster showed a higher catalytic activity than that of Au_{25} nanocluster, similar to the previous results for hydroxyapatite-supported gold nanoclusters towards cyclohexane oxidation [47] and glutathione-coated gold nanoclusters towards benzaldehyde hydrogenation [50]. Therefore, the maximum catalytic activity of dodecanethiolate-coated AuNPs towards silane alcoholysis reactions requires an AuNP size above 1 nm. In contrast to the dodecanethiolate-coated Au_{25} nanocluster, the glutathione-coated Au_{25} nanocluster showed almost no reactivity. The tripeptidyl glutathiones form a more densely packed reaction field than that of dodecanethiolate, but their hydrogen bonding with the reactant molecules seems insufficient for this reaction. These results revealed that the size-dependent catalytic activity of SAM-coated AuNPs smaller than 2 nm resemble that of the supported AuNPs [4–6,44–51], suggesting that the reaction acceleration effect with the SAM is minor in this size range. This is similar to the reported chemoselectivity improvement by the SAM in the hydrogenation and deoxyhydrogenation reactions [20,21].

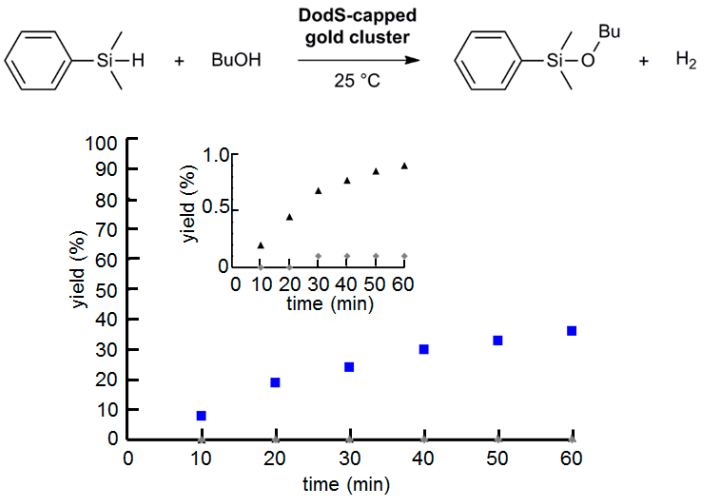

Figure 7. Time-course reaction profile of thiolated gold nanoclusters towards silane alcoholysis. Black triangle: $Octyl_4N[Au_{25}(SDod)_{18}]$, gray diamond: $Na[Au_{25}(SG)_{18}]$, and blue square: $Au_{38}(SDod)_{24}$. Reaction condition: DMPS (150 umol), BuOH (3.0 mL), and gold nanoclusters (0.08 mol %) at 25 °C. The inset is a magnified portion at lower reaction yields.

The catalytic activity of dodecanethiolate SAM-functionalized AuNP-arrays was also evaluated by the catalytic butanolysis reaction of DMPS (Table 1, entries 1, 4–7). The average initial reaction rate of each AuNP-array was calculated from the pseudo-first order kinetics of the initial reaction stage for the three batches of catalytic reactions. The amount of surface Au atoms was estimated as mentioned above, and the initial reaction rate per surface Au atom of **5Dod-array**, **9Dod-array**, **10Dod-array**, **20Dod-array**, and **40Dod-array** was calculated to be 10.8, 7.15, 7.60, 9.72, and 5.27×10^6 min^{-1} mol^{-1}, respectively. Figure 8 shows the size-dependent catalytic activity of dodecanethiolate-functionalized AuNP-arrays. Like the well-known size effect in supported AuNPs [2,3,21], the catalytic activity here increases with the decreasing AuNP size, except for an unexpected increment at around 20 nm. This unique catalytic enhancement for mid-size AuNPs is considered to originate from the combination of size-dependent catalytic activity of supported AuNPs themselves and the reaction acceleration with the alkanethiolate SAM. It is widely accepted that the relative surface ratio of flat planes (terrace site) in AuNPs increases when their size exceeds 5 nm, which agrees with the normal size effect for the catalytic activity of AuNPs decreasing with increasing flat planes [4–6,44–51]. The normal size effect is observed from catalytic silane alcoholysis reactions using immobilized AuNPs and Au thin films without the SAM in the reaction (Figure S9). However, Medlin et al. reported that the terrace sites are the major reactive surfaces of alkanethiolate SAM-capped PdNPs over 5 nm for the hydrogenation of furfural rather than step or defect sites [23]. As similar to the Medlin's report, terrace sites are considered to be the major reactive surfaces for the SAM-capped AuNPs. In the smaller AuNP size range, the effect of the SAM is negligible, and the catalytic activity mainly depends on the size-dependent catalytic activity of AuNP itself, as observed from gold nanoclusters (Figure 7). Contrastingly, in the larger AuNP size range, as represented by the Au thin film, the catalytic activity of the Au surface is quite low, but is enhanced slightly by the SAM (Figure S9) [59]. In the mid-size AuNPs, the surface of AuNPs is composed of flat planes connected with edge atoms, which enables SAMs to have a more dynamic nature than those on the thin film, thus the reaction can be remarkably enhanced with intermolecular interactions between SAMs and reactant molecules. The stronger intermolecular interactions of the SAM in the mid-size AuNPs are represented by the phase-segregated structure of the SAM on AuNPs [60], which makes the mid-size AuNPs more suitable for encapsulating reactant molecules inside the SAM, thus accelerating the catalytic reaction. However, with increasing the size to larger than 20 nm, the surface ratio of flat planes increases, which enables SAMs to lose the flexibility similarly to those on thin film, thus the reaction enhancement effect of the SAM decreases. This novel size effect is considered a unique characteristic of the SAM-capped MNPs.

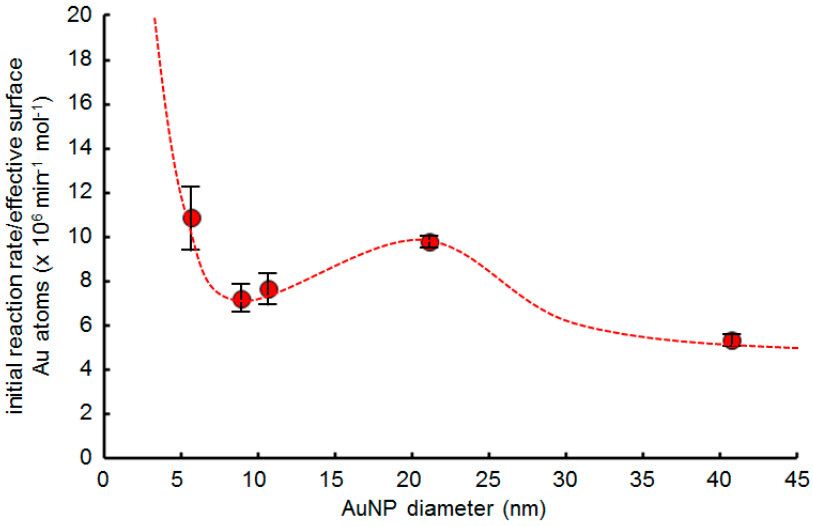

Figure 8. Size dependence of the catalytic activity of dodecanethiolate SAM-functionalized AuNP-arrays.

2.6. Infrared (IR) RA Analysis for the Conformational Change of SAM during the Reaction

For the larger SAM-coated AuNPs, a structural rearrangement of the SAM is needed for the encapsulation of molecules in the SAM. To understand the structural change of the SAM during the catalytic reaction, its structure was analyzed by IR RA measurements. As discussed above, the major reactive surface of SAM-coated AuNPs is considered as the SAM-coated flat Au planes. Thus, flat Au films can be used to model AuNPs over 10 nm in size. In fact, we previously reported a similar temperature-dependent reaction acceleration behavior of SAMs on the Au film compared to those on 10 nm AuNP-arrays in catalytic silane alcoholysis reactions [29]. Here, a dodecanethiolate SAM-functionalized Au film (**Dod-Au**) on a quartz plate was used as the model catalyst. The **Dod-Au** plates were immersed in an EtOH or DMPS solution in EtOH (20 mM) and stood until the DMPS was completely converted to DMPS–OEt, as checked by the GC analysis. The IR RA spectrum of the as-prepared **Dod-Au** is represented by the black line in Figure 9a,b. The C–H stretching vibration region (3000–2800 cm^{-1} in Figure 9b) has the characteristic feature of highly ordered alkyl chains, i.e., the alkyl chains almost stand perpendicularly on the surface [61]. In addition, the methylene d^+ and d^- stretching bands appear at 2849 and 2919 cm^{-1}, respectively, indicating that the alkyl chains are highly packed with all-*trans* zigzag conformations (crystalline state) [62]. After an immersion in EtOH, the crystalline state of the dodecanethiolate SAM was not changed, although the appearance of strong C–O stretching around 1008 cm^{-1} indicates the surface-bound EtOH (Figure 9a, blue line). After the catalytic silane alcoholysis reaction was complete, an obvious structural change of SAM was observed in the spectrum. The dodecanethiolate SAM showed a slightly disordered conformation after the reaction, since the d^+ and d^- bands at 2856 and 2925 cm^{-1} shifted to 2849 and 2919 cm^{-1} in the original crystalline state (Figure 9b, red line). This change is attributed to the silane alcoholysis reaction that took place inside the SAM. Most importantly, small new peaks and shoulder peaks were observed after the reactions at 740, 781, 829, 1114, 1251, 1386, 1429, 3052, and 3070 cm^{-1}, which correspond well to vibration bands of the silylether product DMPS–Oet (Figure 9a,b, green line) and indicate the entrapment of products inside the SAM. This result strongly suggests that the catalytic alcoholysis of DMPS starts with the entrapment of DMPS in the SAM, accompanied by a conformational change of the SAM. Then, the alcoholysis reaction takes place at the surface of AuNPs. During the catalytic reaction, the entrapped product can be replaced by new DMPS molecules. Finally, after completion of the reaction, the remaining DMPS–Oet inside the SAM is not released without the DMPS.

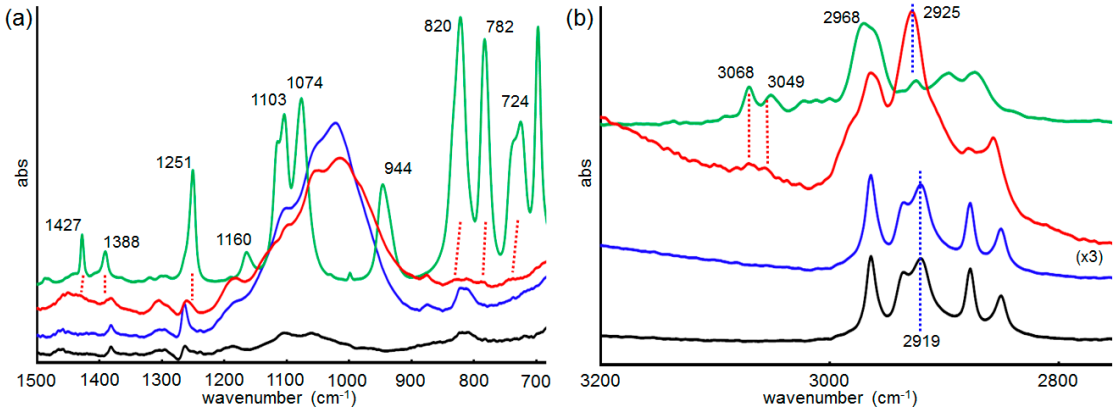

Figure 9. Infrared (IR) reflection–absorption (RA) spectra of **Dod-Au** (black line), **Dod-Au** after immersion in EtOH for 24 h (blue line), **Dod-Au** after immersion in EtOH with DMPS (red line), and the attenuated total reflection (ATR) spectrum of DMPS–OEt (green line) in the (**a**) 700–1500 cm^{-1} and (**b**) 2800–3100 cm^{-1} regions.

In contrast, the IR RA spectrum of the **Dod-Au** immersed in HexOH with DMPS (20 mM) showed similar disorder in the SAM after the catalytic reaction, but there were no vibration bands

that could be attributed to the product. This result suggests that HexOH has a higher affinity for the dodecanethiolate SAM than EtOH due to the longer alkyl chain, thus the product generated inside the SAM was replaced by HexOH molecules, while the disordered conformation of SAM was maintained. A higher affinity of HexOH was also previously observed in the competitive reaction in a mixed alcohol solvent (EtOH:BuOH:HexOH = 1:1:1 in mol), giving DMPS–OHex prior to DMPS–OBu and DMPS–OEt [29].

From these results, we propose a mechanism for the alcoholysis reaction of hydrosilanes catalyzed by SAM-functionalized AuNPs in Figure 10. In the alcohol solvent, the SAM on AuNPs has a highly ordered conformation (depicted as **A** in Figure 10). The intermolecular interaction between the SAMs and hydrosilanes in the polar alcohol solvent enables the entrapment of hydrosilanes inside the SAM, along with a conformational change of the SAM to give the intermediate **B**. Next, the Si–H bond of the entrapped hydrosilane is oxidatively added to the surface of AuNPs, then the excess alcohol molecules smoothly undergo the steps of adsorption and silylether formation, accelerated by charge transfers from the conductive film support (Figure 6) to afford the alcoholysis product inside the SAM (shown as the intermediate **C**). In alcohol solvents with short alkyl chains, such as EtOH, the weaker interaction between the alcohol and SAM only facilitates the replacement of the entrapped C by the reactant hydrosilane molecules to directly regenerate intermediate **B**. Thus, after the reaction was completed, intermediate **C** was observed as the resting state according to the IR RA data (Figure 9). Contrarily, in alcohol solvents with longer alkyl chains, such as HexOH, the stronger interaction between alcohol and SAM leads to the replacement of the entrapped product by alcohol molecules, giving the intermediate **D**. On the other hand, when there are reactant molecules, they are entrapped inside the SAM of **D** by intermolecular interactions to enable the turnover of the catalytic cycle, even though the reaction rate is slower than those in alcohols having shorter alkyl chains, as observed in the previous paper [29].

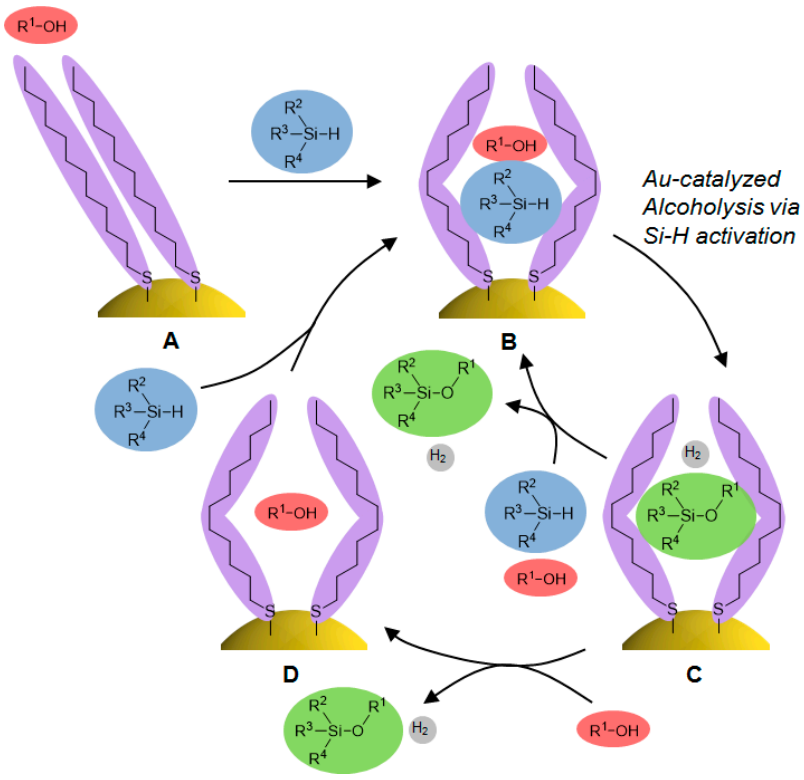

Figure 10. Proposed mechanism of catalytic alcoholysis of hydrosilanes over SAM-functionalized AuNPs.

3. Materials and Methods

3.1. General

UV-Vis extinction spectra were measured on a JASCO V-670 instrument (Tokyo, Japan). Scanning electron microscopy (SEM) observations were carried out on a Hitachi S-4800 microscope (Tokyo, Japan) without a spattering of metals. Gas chromatography (GC) analysis was performed on a Shimadzu GC-2014 instrument (Kyoto, Japan) using a RESTEK Capillary Column Rxi-5ms (30 m × 0.25 mm × 0.25 μm). GC-mass spectrometry (electron ionization) analyses were performed on a Shimadzu GCMS-QP5050 system (Kyoto, Japan). Column chromatography was carried out on silica gel (Kanto Kagaku, Tokyo, Japan, silica gel 60N). ^{1}H and ^{13}C NMR spectra were recorded on JEOL JNM-AL300 and ECS-400 spectrometers (Tokyo, Japan), using $CDCl_3$ or CD_3OD as solvents and tetramethylsilane as an internal standard. The chemical shifts (δ) were expressed in parts per million downfield from tetramethylsilane. The IR attenuated total reflection (ATR) spectra were recorded on JASCO FT/IR-460 Plus and a PerkinElmer Spectrum One FT-IR spectrometers (Waltham, MA, USA). The IR RA measurements [61] were performed on a Magna550 FT-IR spectrometer (Thermo Fischer Scientific, Madison, WI, USA) equipped with a Harrick (Pleasantville, NY) VR1-NIC variable angle reflection accessory mounted with a Harrick PWG-UIR wire-grid polarizer for passing the p-polarization only.

3.2. Materials

Plastic formed carbon (PFC) electrodes were purchased from Tsukuba Materials Information Laboratory Ltd (Ibaraki, Japan). and used after cutting and cleaning by sonication in water and hexane. All organic reagents were purchased from Sigma-Aldrich (St. Louis, MO, USA), Tokyo Chemical Industry (Tokyo, Japan), and Nacalai Tesque (Kyoto, Japan). Dimethylphenylsilane (DMPS) was used without further purification, and all the alcohols were dried over molecular sieves 3A. The AuNPs were synthesized according to the literature methods [30,31] and used after purification by centrifugation. A commercially available AuNP (9 nm diameter, Funakoshi) colloid was used as received. Based on the procedures from our previous papers [32–34], Au-, Cr-, and indium tin oxide (ITO)-spattered quartz plates were functionalized by 1,6-hexanedithiol, and used for the preparation of AuNP-arrays.

3.3. Preparation of AuNP-Arrays

The thiolate-terminated conductive film-coated quartz plate and PFC plate (10 mm × 10 mm × 1.0 mm) were connected to a DC source using gold clips as the cathode and anode. The two electrodes were positioned in parallel to each other with a distance of 1.2 mm between them and immersed in the reaction vessel charged with an alkanethiolate-coated AuNP colloidal solution. Then, a DC voltage was applied at RT while the cap of the vessel was left open. After the complete evaporation of the solvent, the cathode was annealed at 50 °C for 12 h on a hot plate (Model PC-420D, AS-ONE). The annealed quartz plate was washed by sonication in hexane for 1 min, and then dried with nitrogen blowing to produce the AuNP-array on the support. SEM measurements confirmed the formation of regular hexagonal AuNP-arrays. The average coverage of AuNP-arrays was obtained by SEM measurements at 7 points on the substrate, as shown in the previous paper [34].

3.4. Typical Reaction Procedure for AuNP-Array Catalysts

A quartz plate with a supported AuNP-array (1.0 cm × 1.0 cm) was hung by a Teflon-coated wire in a reaction vessel and immersed completely in the alcohol (3.0 mL). Then, a hydrosilane (150 μmol) was added, and the reaction mixture was stirred in a temperature-fixed water bath. The yield was determined by GC analysis. All reaction products were reported in the literature [29], and all reaction yields were averaged from 3 experiments.

3.5. Typical Reaction Procedure for Colloidal AuNP Catalysts

A colloidal solution of AuNPs dispersed in hexane was prepared at a concentration of 2.7×10^{11}/mL, a similar amount of particles to **10Dod-array**, by checking the concentration with UV-visible extinction spectra. The colloidal AuNP solution with the fixed concentration was centrifuged and dried in a vacuum to remove the solvent. The dried AuNPs were dispersed in alcohol (3.0 mL) by sonication, and hydrosilane (150 μmol) was added into the solution. The colloidal solution was stirred in a temperature-fixed water bath. The yield was determined by GC analysis. All reaction yields were averaged from three experiments.

3.6. Preparation of Dodecanethiolate SAM-Functionalized Au Substrate (Dod-Au) for RA IR Measurements

Dodecanethiolate SAM-functionalized Au films (**Dod-Au**) were prepared according to the previous method [29] using Au-sputtered quartz plates (Au thickness: ca 300 nm, quartz: 20 mm × 40 mm × 1 mm). The **Dod-Au** plates were immersed in an EtOH, HexOH, DMPS (20 mM) solution in EtOH, or HexOH. After the complete conversion of DMPS to DMPS–OEt or DMPS–OHex as confirmed by GC analysis, the plates were taken from the vessel, washed with the corresponding alcohol solvents, and dried in a vacuum.

4. Conclusions

The relationship between the reaction acceleration effect with SAM and structural parameters of SAM-functionalized AuNP-array catalysts was investigated by preparing a variety of AuNP catalysts. The coverage of AuNPs was found to show a linear dependence to the catalytic activity below 70% coverage by forming small islands of AuNP-arrays. A comparison of the different supports clarified that a conductive film with a lower work function accelerates the target reaction by facilitating the charge transfer from the conductive film to AuNPs through the 1,6-hexanedithiolate SAM. According to the computational study by Bhattacharjee and Datta [43], the observed support effect is due most likely to the lower energy barrier of the O–H bond cleavage of the alcohol substrates, following the oxidative addition of hydrosilanes and adsorption of alcohols onto the surface of SAM-functionalized AuNPs. The alkanethiolate SAM-functionalized AuNP-array catalysts showed an unexpected size dependence: the mid-sized AuNPs (around 20 nm in diameter) showed higher catalytic activities than those of larger and smaller ones. The present study attributes this atypical size-dependent reactivity to the characteristic function of the SAM on MNPs. The attractive intermolecular interaction between the substrates and the alkyl chains in the SAM accelerates the reaction. The intermolecular interaction is at the AuNP size of 20 nm (maximum) because of the flexible conformational change of alkyl chains. On the other hand, when the size of AuNP is below 10 nm, the sparse alkyl chain packing of the SAM lowers the intermolecular interactions to result in a lower acceleration effect. When the size of AuNP exceeds 40 nm, the dense-packing of the alkyl chains hampers the accommodation of the substrates in the SAM. IR RA measurements using dodecanethiolate SAM-functionalized Au films clarified that the conformational change of the dodecyl groups depends on the alkyl chain length of the alcohol substrates during the catalytic silane alcoholysis reaction. This conformational change accelerated the reaction based on molecular encapsulations inside the SAM in the SAM-functionalized mid-sized AuNP catalysts, compared to SAM-functionalized catalysts with smaller NP sizes. We envision that this newly observed size effect will spur the further development of surface-functionalized MNP catalysts which can attain high catalytic activity and selectivity at the same time.

Supplementary Materials: The following are available online at http://www.mdpi.com/2073-4344/10/8/908/s1, Figure S1: Schematic illustration of a 10Dod-array for calculating surface Au atoms, Figures S2–S5: Micrographic images and UV-Vis absorption spectra of AuNPs before and after thiol functionalization, Figure S6: Time-course reaction trace and pseudo-first order dependence of the initial reaction steps of 10Dod-array catalysts, Figure S7: ^{1}H NMR spectra of the reaction solution with the colloidal 10Dod-AuNP in CD_3OD, Figure S8: Time-course reaction profile of magic number gold nanoclusters, Table S1: Recyclable catalysis of the 10Dod-array, Figure S9: Size dependence of catalytic activity of AuNP-arrays and Au films with or without the dodecanethiolate SAM,

Figure S10: IR ATR spectra of dedocanethiolate SAM-coated AuNPs, Table S2: Catalytic reaction with sterically hindered thiolate-coated AuNP-arrays, Figure S11: SEM image of 10tDod-array, Figure S12: DFT-calculated vibrational bands of DMPS–OEt and proposed conformational change of the SAM, Figure S13: IR RA spectra of Dod-Au substrate in HexOH with DMPS.

Author Contributions: Conceptualization, K.I. (Katsuhiro Isozaki) and K.M.; experiments, T.T. and K.I. (Kosuke Ishibashi); gold nanocluster synthesis, W.K. and Y.N.; RA IR measurement, T.S. and T.H.; writing—original draft preparation, K.I. (Katsuhiro Isozaki); writing—review and editing, K.I. (Katsuhiro Isozaki) and M.N.; funding acquisition, T.T., K.I. (Katsuhiro Isozaki), K.M., and M.N. All authors have read and agreed to the published version of the manuscript.

Funding: This research was financially supported in part by the Japan Society for the Promotion of Science (JSPS) and the Ministry of Education, Culture, Sports, Science and Technology of Japan (MEXT) with JSPS/MEXT KAKENHI Grant numbers JP16805188, JP24656040, JP22106545, JP24106746, and JP30455274, and the Collaborative Research Program of the Institute for Chemical Research (Grant Numbers 2012-14, 2014-16, and 2015-17).

Acknowledgments: T.T. thanks the Japan Society for the Promotion of Science for a Young Scientist Fellowship. K.I. is grateful to T. Bürgi (Université de Genève) for the helpful discussion. SAXS measurements were performed at BL40B2, SPring-8, with the approval of the Japan Synchrotron Radiation Research Institute (JASRI) (Grant Nos. 2010B1744, 2012A1575). This work was supported in part by the Joint Usage/Research Center (JURC) at the ICR, Kyoto University.

Conflicts of Interest: The authors declare no conflict of interest.

References and Notes

1. Liu, L.; Corma, A. Metal catalysts for heterogeneous catalysis: From single atoms to nanoclusters and nanoparticles. *Chem. Rev.* **2018**, *118*, 4981–5079. [CrossRef]
2. Cong, H.; Porco, J.A., Jr. Chemical synthesis of complex molecules using nanoparticle catalysis. *ACS Catal.* **2012**, *2*, 65–70. [CrossRef]
3. Corma, A.; Garcia, H. Supported gold nanoparticles as catalysts for organic reactions. *Chem. Soc. Rev.* **2008**, *37*, 2096–2126. [CrossRef]
4. Yamazoe, S.; Koyasu, K.; Tsukuda, T. Nonscalable oxidation catalysis of gold clusters. *Acc. Chem. Res.* **2014**, *47*, 816–824. [CrossRef]
5. Taketoshi, A.; Haruta, M. Size- and structure-specificity in catalysis by gold clusters. *Chem. Lett.* **2014**, *43*, 380–387. [CrossRef]
6. Haruta, M. Size- and support-dependency in the catalysis of gold. *Catal. Today* **1997**, *36*, 153–166. [CrossRef]
7. Chavda, N.; Trivedi, A.; Thakarda, J.; Agrawal, Y.K.; Maity, P. Size specific activity of polymer stabilized gold nanoparticles for transfer hydrogenation catalysis. *Catal. Lett.* **2016**, *146*, 1331–1339. [CrossRef]
8. Yao, Q.; Wang, C.; Wang, H.; Yan, H.; Lu, J. Revisiting the au particle size effect on TiO_2-Coated Au/TiO_2 catalysts in CO oxidation reaction. *J. Phys. Chem. C* **2016**, *120*, 9174–9183. [CrossRef]
9. Hartadi, Y.; Widmann, D.; Behm, R.J. CO_2 hydrogenation to methanol on supported au catalysts under moderate reaction conditions: Support and particle size effects. *ChemSusChem.* **2015**, *8*, 456–465. [CrossRef] [PubMed]
10. Donoeva, B.G.; Ovoshchnikov, D.S.; Golovko, V.B. Establishing a Au nanoparticle size effect in the Oxidation of Cyclohexene using gradually changing Au catalysts. *ACS Catal.* **2013**, *3*, 2986–2991. [CrossRef]
11. Hartfelder, U.; Kartusch, C.; Makosch, M.; Rovezzi, M.; Sá, J.; van Bokhoven, J.A. Particle size and support effects in hydrogenation over supported gold catalysts. *Catal. Sci. Technol.* **2013**, *3*, 454–461. [CrossRef]
12. Ousmane, M.; Liotta, L.F.; Pantaleo, G.; Venezia, A.M.; Carlo, G.D.; Aouine, M.; Retailleau, L.; Giroir-Fendler, A. Supported Au catalysts for propene total oxidation: Study of support morphology and gold particle size effects. *Catal. Today* **2011**, *176*, 7–13. [CrossRef]
13. Laoufi, I.; Saint-Lager, M.-C.; Lazzari, R.; Jupille, J.; Robach, O.; Garaudée, S.; Gabailh, G.; Dolle, P.; Cruguel, H.; Bailly, A. Size and catalytic activity of supported gold nanoparticles: An in pperando study during CO oxidation. *J. Phys. Chem. C* **2011**, *115*, 4673–4679. [CrossRef]
14. Baiker, A. Crucial aspects in the design of chirally modified noble metal catalysts for asymmetric hydrogenation of activated ketones. *Chem. Soc. Rev.* **2015**, *44*, 7449–7464. [CrossRef] [PubMed]
15. Zaera, F. Regio-, Stereo-, and enantioselectivity in hydrocarbon conversion on metal surfaces. *Acc. Chem. Res.* **2009**, *42*, 1152–1160. [CrossRef]

16. Blaser, H.-U.; Studer, M. Cincona-modified platinum catalysts: From ligand acceleration to technical processes. *Acc. Chem. Res.* **2007**, *40*, 1348–1356. [CrossRef]
17. Bürgi, T.; Baiker, A. Heterogeneous enantioselective hydrogenation over cincona alkaloid modified platinum: Mechanistic insights into a complex reaction. *Acc. Chem. Res.* **2004**, *37*, 909–917. [CrossRef]
18. Hutchings, G.J. New approaches to rate enhancement in heterogeneous catalysis. *Chem. Commun.* **1999**, 301–306. [CrossRef]
19. Liu, P.; Qin, R.; Fu, G.; Zheng, N. Surface coordination chemistry of metal nanomaterials. *J. Am. Chem. Soc.* **2017**, *139*, 2122–2131. [CrossRef]
20. Schoenbaum, C.A.; Schwartz, D.K.; Medlin, J.W. Controlling the surface environment of heterogeneous catalysts using self-assembled monolayers. *Acc. Chem. Res.* **2014**, *47*, 1438–1445. [CrossRef]
21. Kumar, G.; Lien, C.-H.; Janik, M.J.; Medlin, J.W. Catalytic site selction via control over noncovalent interactions in self-assembled monolayers. *ACS Catal.* **2016**, *6*, 5086–5094. [CrossRef]
22. Kahsar, K.R.; Schwartz, D.K.; Medlin, J.W. Control of metal catalyst selectivity through specific noncovalent molecular interactions. *J. Am. Chem. Soc.* **2014**, *136*, 520–526. [CrossRef] [PubMed]
23. Pang, S.H.; Shoenbaum, C.A.; Schwartz, D.K.; Medlin, J.W. Directing reaction pathways by catalyst active-site selection using self-assembled monolayers. *Nat. Commun.* **2013**, *4*, 3448. [CrossRef] [PubMed]
24. Marshall, S.T.; O'Brien, M.; Oetter, B.; Corpuz, A.; Richards, R.M.; Schwartz, D.K.; Medlin, J.W. Controlled selectivity for palladium catalysts using self-assembled monolayers. *Nat. Mater.* **2010**, *9*, 853–858. [CrossRef]
25. Kwon, S.G.; Krylova, G.; Sumer, A.; Schwartz, M.M.; Bunel, E.E.; Marshall, C.L.; Chattopadhyay, S.; Lee, B.; Jellinek, J.; Shevchenko, E.V. Capping ligands as selectivity switchers in hydrogenation reactions. *Nano Lett.* **2012**, *12*, 5382–5388. [CrossRef]
26. Moreno, M.; Kissell, L.N.; Jasinski, J.B.; Zamborini, F.P. Selectivity and reactivity of alkylamine- and alkanethiolate-stabilized Pd and PdAg nanoparticles for hydrogenation and isomerization of allyl alcohol. *ACS Catal.* **2012**, *2*, 2602–2613. [CrossRef]
27. Sadeghmoghaddam, E.; Gu, H.; Shon, Y.-S. Pd nanoparticle-catalyzed isomerization vs hydrogenation of allyl alcohol: Solvent-dependent regioselectivity. *ACS Catal.* **2012**, *2*, 1838–1845. [CrossRef]
28. Wu, B.; Huang, H.; Yang, J.; Zheng, N.; Fu, G. Selective hydrogenation of α,β-unsaturated aldehydes catalyzed by amine-capped platinum-cobalt nanocrystals. *Angew. Chem. Int. Ed.* **2012**, *51*, 344–3443. [CrossRef]
29. Taguchi, T.; Isozaki, K.; Miki, K. Enhanced catalytic activity of self-assembled-monolayer-capped gold nanoparticles. *Adv. Mater.* **2012**, *24*, 6462–6467. [CrossRef]
30. Jana, N.R.; Gearheart, L.; Murphy, C.J. Seeding growth for size control of 5–40 nm diameter gold nanoparticles. *Langmuir* **2001**, *17*, 6782–6786. [CrossRef]
31. Frens, G. Controlled nucleation for the regulation of the particle size in monodisperse gold suspensions. *Nature* **1973**, *241*, 20–22. [CrossRef]
32. Ochiai, T.; Isozaki, K.; Nishiyama, S.; Miki, K. Enhancement of self-assembly of large (>10 nm) gold nanoparticles on an ITO substrate. *Appl. Phys. Express* **2014**, *7*, 065001. [CrossRef]
33. Ochiai, T.; Isozaki, K.; Pincella, F.; Taguchi, T.; Nittoh, K.; Miki, K. Plasmon-resonant optics on an indium–tin-oxide film for exciting a two-pthoton photochromic reaction. *Appl. Phys. Express* **2013**, *6*, 102001. [CrossRef]
34. Isozaki, K.; Ochiai, T.; Taguchi, T.; Nittoh, K.; Miki, K. Chemical coating of large-area Au nanoparticle two-dimensional arrays as plasmon-resonant optics. *Appl. Phys. Lett.* **2010**, *97*, 221101. [CrossRef]
35. Complete exchange of surface ligands on AuNPs (citrate or ascorbate) with dodecanethiol was confirmed by ATR IR measurement (Figure S10).
36. Michaelson, H.B. The work function of the elements and its periodicity. *J. Appl. Phys.* **1977**, *48*, 4729–4733. [CrossRef]
37. Schlaf, R.; Murata, H.; Kafafi, Z.H. Work function measurements on indium tin oxide films. *J. Electron Spectrosc. Relat. Phenom.* **2001**, *120*, 149–154. [CrossRef]
38. The yields of 1,6-hexanethiolate SAM-capped Au, Cr, and ITO substrates after 1 h reaction were 9, 6, and 4%, respectively. The lower yields with the support films clarify that the catalytic activity of supported AuNPs originates from AuNPs.

39. Fulmer, G.R.; Miller, A.J.M.; Sherden, N.H.; Gottlieb, H.E.; Nudelman, A.; Stoltz, B.M.; Bercaw, J.E.; Goldberg, K.I. NMR chemical shifts of trace impurities: Common laboratory solvents, organics, and gases in deuterated solvents relevant to the organometallic chemist. *Organometallics* **2010**, *29*, 2176–2179. [CrossRef]
40. Dirk, K.; Ulf, H.; Joop, A.P. *Handbook of Homogeneous Hydrogenation*; de Vries, J.G., Elsevier, C.J., Eds.; Wiley-VCH: Weinheim, Germany, 2007; pp. 585–630.
41. Mitsudome, T.; Urayama, T.; Maeno, Z.; Mizugaki, T.; Jitsukawa, K.; Kaneda, K. Highly efficient dehydrogenative coupling of hydrosilanes with amines or amides using supported gold nanoparticles. *Chem. Eur. J.* **2015**, *21*, 3202–3205. [CrossRef]
42. Mitsudome, T.; Yamamoto, Y.; Noujima, A.; Mizugaki, T.; Jitsukawa, K.; Kaneda, K. Highly efficient etherification of silanes by using a gold nanoparticle catalyst: Remarkable effect of O_2. *Chem. Eur. J.* **2013**, *19*, 14398–14402. [CrossRef]
43. Bhattacharjee, R.; Datta, A. Role of carbon support for subnanometer gold-cluster-catalyzed disiloxane synthesis from hydrosilane and water. *J. Phys. Chem. C* **2017**, *121*, 20101–20112. [CrossRef]
44. Li, M.-B.; Tian, S.-K.; Wu, Z.; Jin, R. Cu^{2+} induced formation of $Au_{44}(SC_2H_4Ph)_{32}$ and its high catalytic activity for the reduction of 4-nitrophenol at low temperature. *Chem. Commun.* **2015**, *51*, 4433–4436. [CrossRef] [PubMed]
45. Li, G.; Zeng, C.; Jin, R. Thermally robust $Au_{99}(SPh)_{42}$ nanoclusters for chemoselective hydrogenation of nitrobenzaldehyde derivatives in water. *J. Am. Chem. Soc.* **2014**, *136*, 3673–3679. [CrossRef] [PubMed]
46. Li, G.; Jiang, D.-E.; Kumar, S.; Chen, Y.; Jin, R. Size dependence of atomically precise gold nanoclusters in chemoselective hydrogenation and active site structure. *ACS Catal.* **2014**, *4*, 2463–2469. [CrossRef]
47. Liu, Y.; Tsunoyama, H.; Akita, T.; Xie, S.; Tsukuda, T. Aerobic oxidation of cyclohexane catalyzed by size-controlled Au clusters on hydroxyapatite: Size effect in the Sub-2 nm regime. *ACS Catal.* **2011**, *1*, 2–6. [CrossRef]
48. Negishi, Y.; Nakazaki, T.; Malola, S.; Takano, S.; Niihori, Y.; Kurashige, W.; Yamazoe, S.; Tsukuda, T.; Häkkinen, H. A critical size for emergence of nonbulk electronic and geometric structures in dodecanethiolate-protected Au clusters. *J. Am. Chem. Soc.* **2015**, *137*, 1206–1212. [CrossRef] [PubMed]
49. Zhu, M.; Aikens, C.M.; Hollander, F.J.; Schatz, G.C.; Jin, R. Correlating the crystal structure of a thiol-protected Au_{25} cluster and optical properties. *J. Am. Chem. Soc.* **2008**, *130*, 5883–5885. [CrossRef]
50. Heaven, M.W.; Dass, A.; White, P.S.; Holt, K.M.; Murray, R.W. Crystal structure of the gold nanoparticle $[N(C_8H_{17})_4][Au_{25}(SCH_2CH_2Ph)_{18}]$. *J. Am. Chem. Soc.* **2008**, *130*, 3754–3755. [CrossRef]
51. Negishi, Y.; Chaki, N.K.; Shichibu, Y.; Whetten, R.L.; Tsukuda, T. Origin of Magic stability of thiolated gold clusters: A case study on $Au_{25}(SC_6H_{13})_{18}$. *J. Am. Chem. Soc.* **2007**, *129*, 11322–11323. [CrossRef]
52. Dolaminc, I.; Knoppe, S.; Dass, A.; Bürgi, T. First enantioseparation and circular dichroism spectra of Au_{38} clusters protected by achiral ligands. *Nat. Commun.* **2012**, *3*, 1802.
53. Qian, H.; Zhu, M.; Anderson, U.N.; Jin, R. Facile, large-scale synthesis of dodecanethiol-stabilized Au_{38} clusters. *J. Phys. Chem. A* **2009**, *113*, 4281–4284. [CrossRef]
54. Chaki, N.K.; Negishi, Y.; Tsunoyama, H.; Shichibu, Y.; Tsukuda, T. Ubiquitous 8 and 29 kDa Gold: Alkanethiolate cluster compounds: Mass-Spectrometric determination of molecular formulas and structural implications. *J. Am. Chem. Soc.* **2008**, *130*, 8608–8610. [CrossRef] [PubMed]
55. Donkers, R.L.; Lee, D.; Murray, R.W. Synthesis and isolation of the molecule-like cluster $Au_{38}(PhCH_2CH_2S)_{24}$. *Langmuir* **2004**, *20*, 1945–1952. [CrossRef]
56. Shichibu, Y.; Negishi, Y.; Tsukuda, T.; Teranishi, T. Large-Scale synthesis of thiolated Au_{25} clusters via ligand exchange reactions of phosphine-stabilized Au_{11} clusters. *J. Am. Chem. Soc.* **2005**, *127*, 13464–13465. [CrossRef] [PubMed]
57. Negishi, Y.; Takasugi, Y.; Sato, S.; Yao, H.; Kimura, K.; Tsukuda, T. Magic-numbered Au_n clusters protected by glutathione monolayers (n = 18, 21, 25, 28, 32, 39): Isolation and spectroscopic characterization. *J. Am. Chem. Soc.* **2004**, *126*, 6518–6519. [CrossRef]
58. The respective core size of [Au25SR18]− and Au38SR24 clusters is ca. 1.0 [47] and 1.1 nm [55] from TEM.
59. Reaction yield: 6.7% (Au thin film) and 8.7% (Dod-Au thin film) [29]. The slightly increased yield by SAM functionalization clarifies the reaction acceleration effect of SAMs even on the flat Au surface.
60. Ghorai, P.K.; Glotzer, S.C. Molecular dynamics simulation study of self-assembled monolayers of alkanethiol surfactants on spherical gold nanoparticles. *J. Phys. Chem. C* **2007**, *111*, 15857–15862. [CrossRef]

61. Hasegawa, T. *Quantitative Infrared Spectroscopy for Understanding of a Condensed Matter*; Springer: Berlin/Heidelberg, Germany, 2017.
62. Hostetler, M.J.; Stokes, J.J.; Murray, R.W. Infrared spectroscopy of three-dimensional self-assembled monolayers: *N*-alkanethiolate monolayers on gold cluster compounds. *Langmuir* **1996**, *12*, 3604–3612. [CrossRef]